Mechanism of asymmetric lineshape broadening in $GaAs_{1-x}N_x$ Raman spectra

Aleksej Mialitsin,* Brian Fluegel, Aaron Ptak, and Angelo Mascarenhas
National Renewable Energy Laboratory, 15013 Denver West Parkway, Golden, Colorado 80401, USA
(Received 14 March 2012; revised manuscript received 15 May 2012; published 19 July 2012)

Resonance Raman spectroscopy is used to probe the asymmetric broadening of the LO phonon linewidth in a dilute $GaAs_{1-x}N_x$ alloy ($x = 0.41\%$). Electronic Raman scattering from a broad continuum is observed that gets enhanced concurrently with the LO phonon linewidth under resonance. The Fano interaction between the LO phonon and the electronic continuum is used to develop a model that satisfactorily explains the origin of the asymmetric LO phonon linewidth broadening in this abnormal alloy as arising due to coupling between the discrete and the continuum configurations.

DOI: 10.1103/PhysRevB.86.045209 PACS number(s): 78.30.−j, 63.20.kp, 63.50.−x

I. INTRODUCTION

In the Raman spectra of ternary semiconductor alloys, a broadening of the LO phonon linewidth occurs due to alloy disorder. However, in resonant Raman scattering, no excitation energy dependence of the phonon linewidth has been observed for conventional semiconductor alloys. In an earlier Raman study on $GaAs_{1-x}N_x$, we reported a peculiar linewidth broadening for light scattering from LO phonons, finding it to be highly asymmetric towards the low frequency side of the LO Raman line.[1] In consequent studies, resonant Raman scattering experiments, where Raman spectra are recorded as a function of excitation wavelength, a resonance of the asymmetric broadening at two particular energies, E_W and E'_W, has been revealed.[2] It was observed that the excitation profile of the empirically determined full width at half maximum (FWHM) displayed a "camel back" shape. These linewidth resonances were shown to correlate with nitrogen induced changes to the electronic structure of $GaAs_{1-x}N_x$. The "linewidth" of the asymmetric peak was determined on a purely empirical basis with the exact mechanism of broadening remaining unknown.

We now provide a model for the origin of this peculiar linewidth broadening that quantitatively describes the asymmetric lineshape. In this paper, we report the observation of a low energy electronic continuum in the Raman spectra from dilute GaAsN alloy. By systematically focusing on the low frequency region of the resonant Raman spectra, we establish that the asymmetric linewidth broadening of the 295 cm^{-1} GaAs LO phonon is due to the Fano interaction of the continuum with the discrete phonon mode. The coupling parameter determined from the Raman lineshape resonates at the empirically established energy E_W corresponding to the L critical point of the GaAs:N band structure.

II. EXPERIMENTAL METHODS

The GaAs:N sample with 0.41% nitrogen concentration has been grown by molecular-beam epitaxy on a p-type Zn-doped (001) oriented substrate (sample no. EB661).[3] The sample has been cleaved along the [110] and [1$\bar{1}$0] directions and glued to a cold-finger of an Oxford Instruments He-flow cryostat with silver epoxy. A DCM dye laser and a Ti:Si laser were used as the excitation light source for the excitation wave length ranges 640–695 nm and 700–750 nm, respectively. All spectra were taken in the "polarized" optics configuration, which means that laser light was linearly polarized and the polarizing and analyzing elements for the incoming and scattered light were arranged in parallel. The Raman signal was analyzed via a triple-stage Jobin Yvon T64000 spectrometer. Data was captured with a PC controlled Andor silicon CCD.

III. THEORETICAL METHODS

If a discrete mode ϕ couples to a continuum of excitations ψ, quantum interference of wavefunctions leads to asymmetric lineshapes. The analytical expression to describe such lineshapes in condensed matter spectroscopies was suggested by Fano for absorption lines in the ionization continuum of atomic (and molecular) spectra:[4] $I \sim |\langle\Psi_E|T|i\rangle|^2/|\langle\psi_E|T|i\rangle|^2 = (q+\varepsilon)^2/(1+\varepsilon^2)$. The LHS of this equation is the ratio of the excitation probability of the interacting (hybridized) configuration to that of an unperturbed configuration, where $|i\rangle$ denotes the initial state, T a generic transition operator, and the capital and the lower case *bras* are respectively the hybridized and the unperturbed states. The RHS is an effective functional form with an "asymmetry parameter" q related to the coupling strength between the two configurations, and $\varepsilon \equiv \varepsilon(E)$ is a "reduced energy" variable. Later, Klein showed that hybridized continuum-discrete peaks in Raman spectra can be described by exactly the same analytical expression.[5] The spectroscopic lineshape of the hybridized configuration displays an asymmetry on one side of the discrete mode and an antiresonance (reduced intensity) on the other side, as shown in Fig. 1. This occurs because the transition probability from an initial state $|i\rangle$ to a hybridized state $|\Psi\rangle$ can be written as a difference of two terms with orthogonal trigonometric functions (sin and cos). These terms add constructively or destructively, depending on the sign of the wavefunction phase Δ, which changes sign when the excitation frequency crosses a certain resonance frequency. However, both Fano's original and the later description by Klein have the shortcoming of the Dirac-δ-function-like discrete state approximation. Among other things, it forces a complete antiresonance of the hybridized spectral intensity, which is not observed in real spectra. Blumberg *et al.*,[6] and later Mialitsin,[7] have expanded the Fano lineshape treatment of Raman spectra to finite linewidths of the discrete mode. In this case, the Raman response of the hybridized configuration

can be described by a function

$$f(\nu,\omega) \sim \frac{\pi r(\omega)\left[\left((\omega-\omega_{\mathrm{LO}})+\nu\frac{\tau}{t}\right)^2+\gamma_{\mathrm{LO}}(\nu^2\pi r(\omega)+\gamma_{\mathrm{LO}})\right]+\gamma_{\mathrm{LO}}\left(\nu R(\omega)+\frac{\tau}{t}\right)^2}{(\omega-\omega_{\mathrm{LO}}-\nu^2R(\omega))^2+(\nu^2\pi r(\omega)+\gamma_{\mathrm{LO}})^2}, \quad (1)$$

where t and τ, respectively, denote the light interaction strength with the discrete mode and with the continuum of states, ν is the coupling strength between the discrete mode and the continuum, ω_{LO} and γ_{LO} are the frequency and the linewidth of the unperturbed GaAs LO phonon, and $R(\omega)$ and $r(\omega)$ are the real and the imaginary parts of the Green's function generating the continuum in the form $G(\omega) \sim R(\omega) - \imath\pi r(\omega)$. In Fig. 1, we compare the functional form of the expression (1) with that of an unperturbed Raman oscillator[8] on top of a constant continuum [Fig. 1(a)] as well as that of Eq. (1) with the expression of a Dirac-δ-function approximation [Fig. 1(b)]. Both cases are juxtaposed to a sample from experimental data described in the following section. In this paper, we adopt the finite-linewidth treatment provided by Eq. (1), instead of the more commonly used Fano expression parameterized by q and ε. Equation (1) provides a better approximation of the physical system, and, most importantly, it features the coupling strength ν scaled with the ratio of the light interactions strengths, as a fitting parameter to the experimental data. In contrast to a purely phenomenological parameter q, this scaled coupling strength $\tilde{\nu} = \nu \cdot \tau/t$, reflects directly a physical property of the underlying model. Derivation of Eq. (1) and the specific choice of the function $r(\omega)$ approximating a continuum of nearly constant magnitude are described in the Appendix.

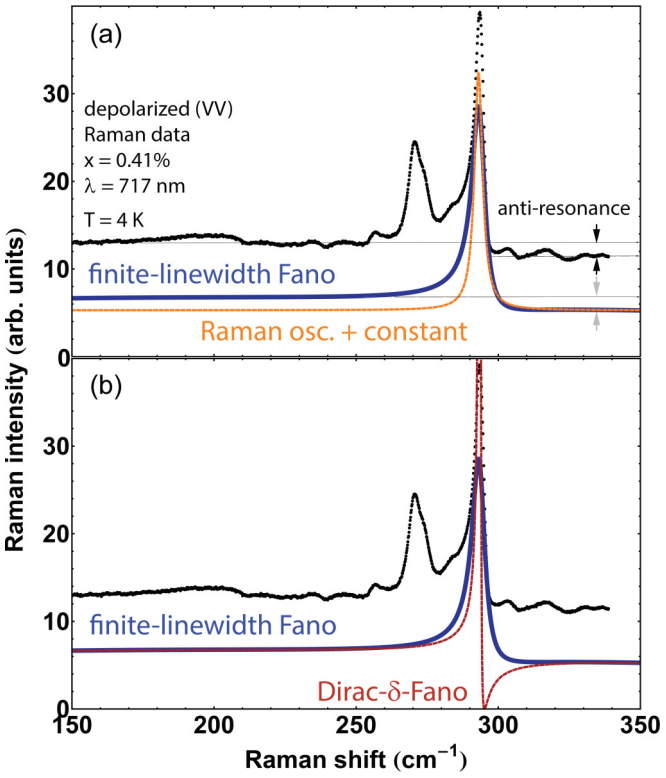

FIG. 1. (Color online) Comparison of the configuration interaction approximated by the "finite linewidth" expression [Eq. (1)] to a bare superposition (a) and (b) to the configuration interaction approximated by the "Dirac-δ-function" expression given by Ref. 5. A set of experimental data is shown for scale.

IV. RESULTS

A. Experimental data

We measure a GaAs:N sample with a nitrogen content of 0.41%, which lies at the lower end of nitrogen concentrations investigated previously with resonance Raman.[2] This is the impurity doping regime, where the E_W and the E'_W linewidth resonances are still well separated, but also one that potentially serves as a good starting point for resonance Raman investigations of the experimentally challenging more dilute regimes. In Fig. 2, we show a sequence of selected Raman spectra from this 0.41% sample. The sequence [Figs. 2(a)–2(d)] is ordered as a function of increasing excitation wavelength (decreasing energy) from 645.1 to 720.1 nm (1.92–1.72 eV). To validate the conjecture of coupled configurations it is necessary to measure the relative light scattering frequencies from 300 cm^{-1}, where the broadened LO-phonon mode is located, down to about 30 cm^{-1}. Previous Raman scattering studies concentrated on the LO phonon frequency, as a function of temperature,[9] concentration,[10] or the low frequency Raman resonances between 1.83 and 1.96 eV excitation energies.[11] To the best of our knowledge, systematic correlations between the low frequency resonances and the LO phonon line shape have not been examined. The 645 nm spectrum shown in Fig. 2(a) exhibits as its main features the slightly asymmetrically broadened LO-phonon peak at 295 cm^{-1} and, adjacent to it, a forbidden TO-phonon peak at 270 cm^{-1} that arises due to lattice-symmetry breaking in the presence of disorder. Both peaks reside noticeably on a broad extended continuous background. These narrow, high intensity peaks are respectively labeled LO and TO in the same panel. The residual background shows two low intensity cusps at about 60 and 210 cm^{-1} labeled as ES$_1$ and ES$_2$, respectively, to reflect their anticipated *electronic scattering* origin. As the excitation wavelength changes, we observe that the residual continuum gets enhanced concomitantly with the broadening of the LO peak. The ES$_1$ and ES$_2$ peaks intensity displays a prominent resonance as a function of wavelength. In addition, while the ES$_2$ peak position remains the same as a function of wavelength, the ES$_1$ peak position moves to higher Raman shifts with increasing wavelength, such that beyond 720 nm [Fig. 2(d)] both peaks almost merge due to accompanying broadening of the features. We link the resonating ES peaks to the interacting part of the continuum, which is treated separately, from the monotonically rising noninteracting part as outlined below. An overview of the intricate resonance pattern of the electronic excitations is presented in Fig. 3.

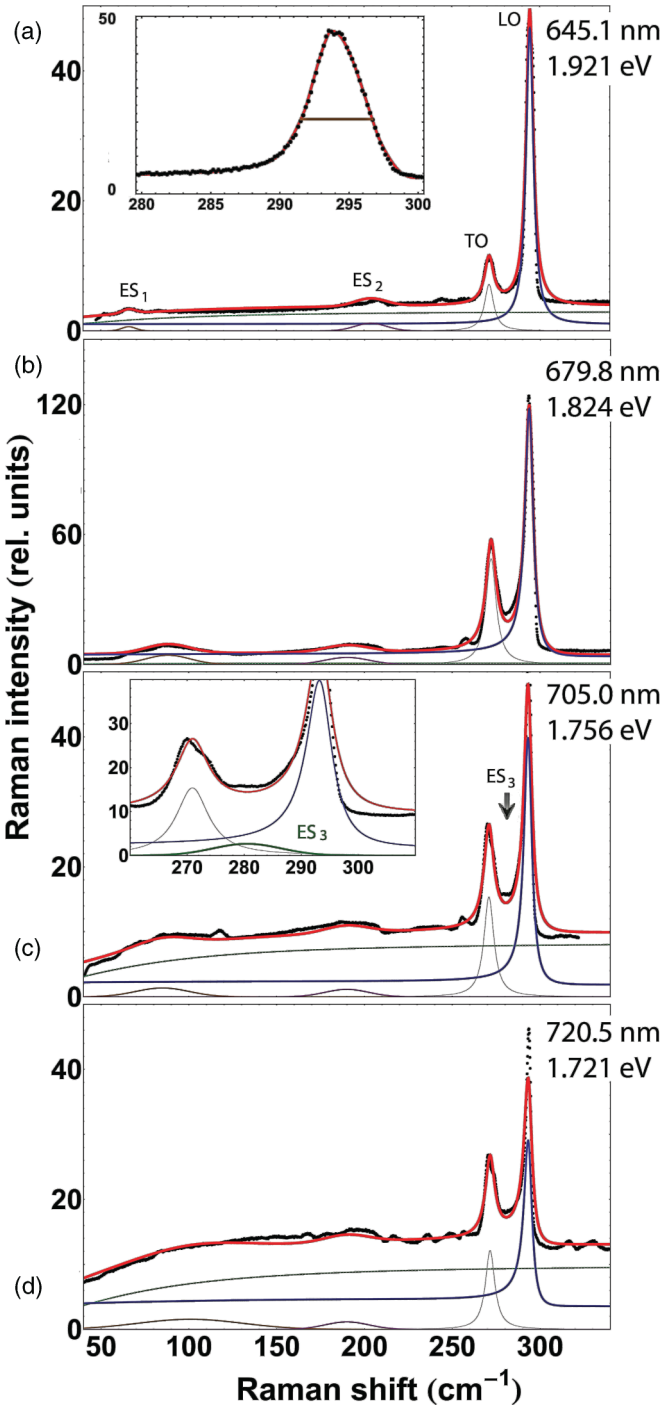

FIG. 2. (Color online) Selected Raman scattering data with the corresponding fits, and the fit decomposition according to Eq. (2): (a)–(d) Sequence of experimental data for increasing wavelengths (decreasing energies) from top to bottom. The inset in (a) shows the empirically determined LO-phonon effective linewidth; the inset in (c) shows the alleged position of the ES_3 resonant electronic scattering band.

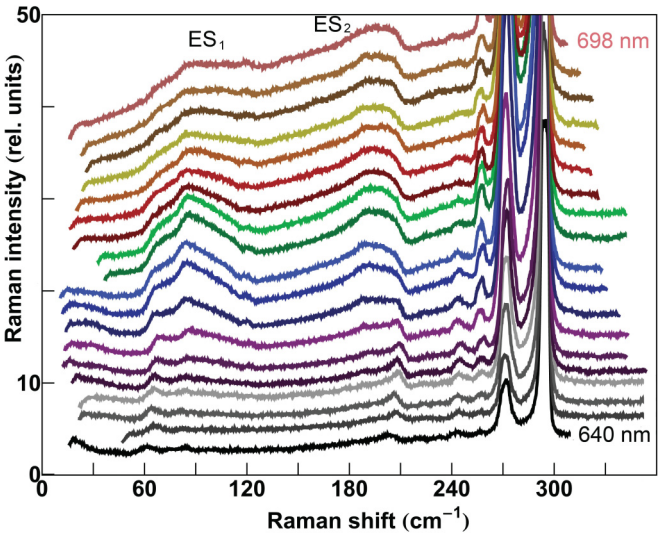

FIG. 3. (Color online) Development of the Raman continuum in the 0.41% GaAs:N between 640 and 700 nm. The line shape changes of the ES bands constitute a unique signature of electronic Raman scattering, see Ref. 12.

B. Configuration interaction model (Fano lineshape)

This correlation of the electronic-continuum resonance and the asymmetric linewidth broadening of the LO phonon immediately presents us with a physical model that we proceed to explore in the following paragraphs. To describe the recorded Raman spectra we devise a model which consists of the superposition of the TO peak modeled with a Raman oscillator,[8] the electronic scattering peaks 1 and 2 modeled by a Gaussian distribution, and the LO-phonon-continuum coupled configuration modeled with the finite-linewidth Fano lineshape [Eq. (1)]:

$$\chi''(\omega) = \text{noninteracting cont.} + \text{TO phonon} + \text{Fano}(\nu) + \text{ES}_1 + \text{ES}_2. \quad (2)$$

As suggested above, the continuum is divided in two parts: the interacting part contained in the Fano-lineshape and the noninteracting part, fitted separately. The noninteracting part originates from the semi-insulating substrate of the sample as has been verified by comparisons with a GaAs:N sample grown on an undoped substrate.[13] The interacting part is included in the configuration interaction and is the one that displays the excitation resonance together with the LO-peak effective linewidth γ_0 and the electronic scattering peaks ES_i. The effective linewidth γ_0, which corresponds to the FWHM measure in Ref. 2, is determined empirically. We draw a smoothed spline function through the data points and evaluate its value at 40% of the peak maximum. The difference between the Raman shifts of the two unique values obtained in such a way on both sides of the peak maximum constitutes the effective linewidth. The fitting model is shown in Fig. 2 with a thick red line that overlaps the data. The respective decompositions are shown underneath: the noninteracting continuum (thin smoothly using line), the noninteracting TO phonon (thin curve at about 270 cm^{-1}), the first electronic continuum peak (thin curve in the 100 cm^{-1} range), the second electronic continuum peak (thin curve in the 200 cm^{-1} range), and the hybridized configuration (thick blue line below the data).

In Fig. 4, we compare the effective linewidth of the broadened LO-phonon (upper panel) with the absolute value

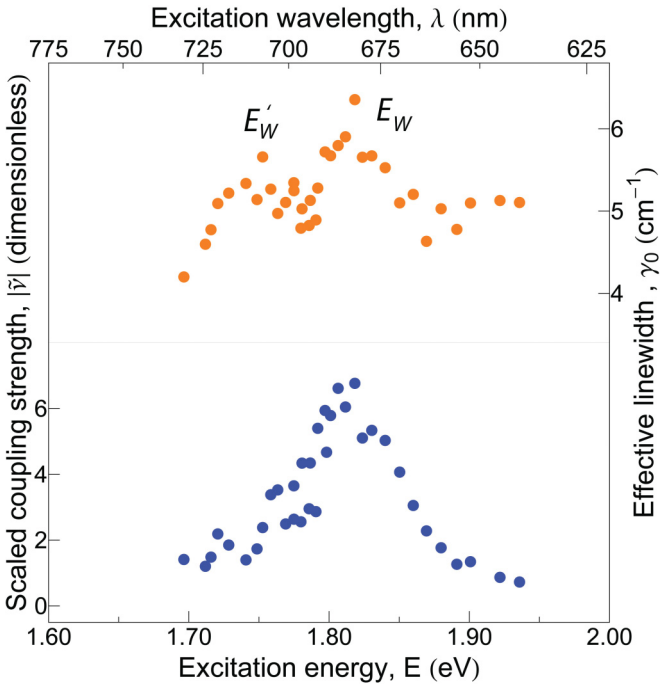

FIG. 4. (Color online) Absolute value of the scaled coupling strength $|\tilde{\nu}| = |\nu \cdot \tau/t|$, determined from the fit, juxtaposed with the effective linewidth γ_0 (full width at 40% max.), determined empirically: upper panel (right scale) refers to γ_0, lower panel (left scale) to $\tilde{\nu}$.

of the scaled coupling strength (lower panel), determined from the fitting model. The scaled coupling strength $\tilde{\nu}$, which is a linearly independent fitting parameter of Eq. (1), is negative throughout all excitation wavelengths reflecting the fact that the LO-phonon couples primarily to continuous transitions at lower energies. This is evident from the fact that the asymmetric broadening occurs towards lower Raman shifts or to the left side of the spectrum. The E_W maximum of the effective linewidth resonance excitation profile at ca. 1.82 eV coincides with the maximum of the scaled coupling strength curve. But the E_W' maximum at about 1.75 eV of the linewidth excitation profile is not reflected in the scaled coupling strength. For this, we offer the following explanation: The effective linewidth is measured only through the Raman intensity at about 290 cm^{-1} in the immediate vicinity of the LO-phonon maximum. The coupling strength, however, is determined through the lineshape of the asymmetrically broadened LO phonon in a wide range of frequencies including the antiresonance dip to the right of the LO-phonon maximum. Therefore, we conclude that the linewidth broadening at E_W corresponds to an all over renormalization of the spectral lineshape reflecting a resonance in the coupling strength. However, the broadening at 1.75 eV corresponds to a local intensity increase at about 290 cm^{-1} without the spectral lineshape renormalization at other frequencies. Since the coupling strength is determined by the overall lineshape extending a few tens of wave numbers to the left and to the right of the LO-phonon peak position, the fitting procedure would not pick up a local broadening occurring only a few wave numbers to the left of the peak. Such a broadening can be produced by a local resonant electronic scattering mode. Indeed, upon a closer look, we see evidence for the presence of such a mode in the raw data, which is indicated by an arrow in Fig. 2(c) and labeled ES_3. By inspection, we find that subtracting a Gaussian mode of the shape $g(\omega) = (\alpha/\sigma\sqrt{\pi/2})\exp[-2(\omega - \omega_{ES_3})^2/\sigma^2]$ with an amplitude α of 40 relative units, a standard deviation σ of 12 cm^{-1}, and a center position ω_{ES_3} of 280 cm^{-1} [Fig. 2(c) inset], reduces the effective linewidth in the 705 nm spectrum by approximately 0.5 cm^{-1}, which is of the same magnitude as the E_W' resonance. We contend that the continuum bands ES_i ($i = 1, 2,$ and 3) arise from hydrogenlike transitions within the bound states formed by trapped nitrogen impurities.[14,15] This means that, at 0.41% nitrogen concentration, the isoelectronic impurity wavefunctions continue to retain some of their local character. This observation of the electronic continuum in GaAs:N is particularly exciting, because in contrast to known reports of Raman excitations from shallow donors in semiconductors like SiC,[16] here, we observe neutral deep impurities in their excited state. Our suggested theoretical model makes it possible to distinguish between the lineshape renormalization due to resonance in the coupling strength of the configurations interaction and an effective linewidth increase due to a local resonance band. From this, it follows that E_W and E_W' resonances of the LO-phonon linewidth broadening in the GaAs:N alloy are of different nature: The E_W resonance arises from the Kohn anomaly in the density of states in the L point of the GaAs Brillouin zone, ca. 1.8 eV above the Γ point of the valency band. An increase in the density of states increases the coupling. In more general terms, E_W is a vestige of a $k \neq 0$ critical point in the Raman response. In the presence of nitrogen impurities, the degeneracy of the L point is broken into a singlet and a triplet state, L_{1c} and L_{3c}.[17] The intensity resonance of the LO-phonon in GaAs:N at E_I has been linked to the singlet state.[2] Here, we find that it is only the E_W linewidth resonance that is linked to the triplet state and is of fundamental electronic structure nature. The E_W' resonance, on the contrary, appears to arise from an impurity-induced electronic scattering band, making it of incidental nature. This, among other things, helps to explain the difference in the magnitude of the two linewidth resonances at higher nitrogen concentrations (Ref. 2, Fig. 1 therein).

V. CONCLUSION

In summary, we have reported an excitation energy resonance in the low Raman shift signal of electronic origin from a dilute GaAs:N alloy with a nitrogen concentration of 0.41%. By fitting the spectral lineshape to the functional form of the continuum-discrete configuration interaction, we have established in a quantitative way that there is *coupling* between the GaAs LO phonon and this continuous Raman signal, which leads to an asymmetric lineshape of the LO phonon and an antiresonance in Raman intensity. The resonant excitation profile of the coupling parameter correlates with the 1.8 eV E_W effective LO-phonon linewidth resonance, which corresponds to the L critical point of the GaAs:N band structure. The E_W' resonance is attributed to an electronic scattering mode resonating at 1.75 eV. Investigation of this resonance behavior towards more dilute nitrogen concentrations is a promising endeavor for future research.

ACKNOWLEDGMENTS

We acknowledge the financial support of the Department of Energy Office of Science under Grant No. DE-AC36-08GO28308. A.M. acknowledges Ilia Slov'yov from Beckman Institute for support with figures layout and automation of data analysis.

APPENDIX

1. Solution of the Dyson equation

The Fano problem of an interacting configuration in Raman scattering can be solved analytically. The transition from the initial state to an excited state is achieved by means of the transition vector

$$\Upsilon = \begin{pmatrix} \tau \\ t \end{pmatrix},$$

where τ denotes the light interaction strength with the discrete mode and t denotes the light interaction strength with the continuum of states. Here, τ and t have to be viewed as phenomenological "effective" interaction strengths that indirectly translate into the respective amplitudes of the continuum portion and the discrete portion of the hybridized Fano response [Eq. (1)]: t determines the asymptotic behavior of the flat portion of the curve and τ determines how high the LO phonon peak spikes above that flat portion. In reality, under resonant Raman light does not interact directly with phonons or other excitations on the energy scale of tens of meV, instead, it causes interband transitions, and the resulting electrons and holes interact with these excitations.

The Raman susceptibility χ'' is calculated as:

$$\chi''(\omega) = -\Im[\Upsilon^\dagger G(\omega)\Upsilon]\,, \tag{A1}$$

where $G(\omega)$ is the Green's function of the interacting system defined through the noninteracting Green's function G_0 and the interaction matrix

$$V = \begin{pmatrix} 0 & \nu \\ \nu^* & 0 \end{pmatrix}$$

as the solution of Dyson's equation:[5]

$$G(\omega) = G_0(\omega) + G_0(\omega)VG(\omega). \tag{A2}$$

Both $G(\omega)$ and $G_0(\omega)$ are 2×2 matrices. Off-diagonal matrix elements are zero for $G_0(\omega)$, with the diagonal elements being the single valued Green's functions of the respective subsystems.

For simplicity, the Green's function of the discrete state is taken to be the one generating the Lorentzian response:

$$d(\omega) = \frac{1}{\omega - \omega_0 + \imath\gamma}\,, \tag{A3}$$

and the continuum Green's function $c(\omega)$ is assumed to be of the general form:

$$c(\omega) \sim R(\omega) - \imath\pi r(\omega)\,. \tag{A4}$$

Given that a Green's function $G(z) = \Re[g(z)] + \imath\Im[g(z)]$ real and imaginary parts are related to each other through the Hilbert transformation:[18]

$$P\int_{-\infty}^{\infty} \frac{\Re[G(z)]}{z-a}dz = -\pi\Im[G(z)] \quad \text{and} \tag{A5}$$

$$P\int_{-\infty}^{\infty} \frac{\Im[G(z)]}{z-a}dz = \pi\Re[G(z)]\,, \tag{A6}$$

the notation of Eq. (A4) allows for a convenient calculation of the real part of the continuum Green's function if the imaginary part has been determined from the experiment:

$$\begin{aligned} R(\omega) = \Re[c(\omega)] &= \frac{1}{\pi}P\int_{-\infty}^{\infty}\frac{\Im[c(\omega')]}{\omega'-\omega}d\omega' \\ &= \frac{1}{\pi}P\int_{-\infty}^{\infty}\frac{-\pi r(\omega')}{\omega'-\omega}d\omega' = -H_T\left[r(\omega)\right]\,, \end{aligned} \tag{A7}$$

where H_T denotes the Hilbert transform. The tradeoff in the above convention is that the rescaling factor of π now appears in the calculation of the imaginary part:

$$\begin{aligned} \pi r(\omega) = -\Im[c(\omega)] &= -\left(-\frac{1}{\pi}\mathcal{P}\int_{-\infty}^{\infty}\frac{\Re[c(\omega')]}{\omega'-\omega}d\omega'\right) \\ &= \frac{1}{\pi}H_T\left[R(\omega)\right]\,. \end{aligned} \tag{A8}$$

Since it is the imaginary part $\pi r(\omega)$ that is obtained by Raman scattering, this latter inverse transformation [Eq. (A8)] is not used in the following derivations. Solving Eq. (A2) for $G(\omega)$ gives

$$G(\omega) = (1 - G_0(\omega)V)^{-1}G_0(\omega)\,. \tag{A9}$$

Here, we work with

$$G_0 = \begin{pmatrix} d(\omega) & 0 \\ 0 & c(\omega) \end{pmatrix} \quad \text{and} \quad V = \begin{pmatrix} 0 & \nu \\ \nu & 0 \end{pmatrix}, \quad \nu \in \mathbb{R}.$$

Since the inverse of a 2×2 matrix

$$A = \begin{pmatrix} a_{11} & a_{12} \\ a_{21} & a_{22} \end{pmatrix},$$

is

$$\begin{aligned} A^{-1} &= \frac{1}{a_{11}a_{22} - a_{12}a_{21}}\begin{pmatrix} a_{22} & -a_{12} \\ -a_{21} & a_{11} \end{pmatrix} \\ &= \frac{1}{\det A}\begin{pmatrix} a_{22} & -a_{12} \\ -a_{21} & a_{11} \end{pmatrix}, \end{aligned} \tag{A10}$$

it follows that

$$\begin{aligned} &(1 - G_0(\omega)V)^{-1}G_0(\omega) \\ &\quad= \frac{1}{\det[1 - G_0(\omega)V]}\begin{pmatrix} 1 & \nu d \\ \nu c & 1 \end{pmatrix}\begin{pmatrix} d & 0 \\ 0 & c \end{pmatrix} \\ &\quad= (1 - \nu^2 cd)^{-1}\begin{pmatrix} d & \nu cd \\ \nu cd & c \end{pmatrix}. \end{aligned} \tag{A11}$$

Finally,

$$(\tau \quad t)\begin{pmatrix} d & \nu cd \\ \nu cd & c \end{pmatrix}\begin{pmatrix} \tau \\ t \end{pmatrix} = d\tau^2 + 2\nu cd\tau t + ct^2 \tag{A12}$$

and

$$\begin{aligned} &(1 - \nu^2 c(\omega)d(\omega))^{-1} \\ &\quad= \frac{\omega - \omega_0 + \imath\gamma}{(\omega - \omega_0 - \nu^2 R(\omega)) + \imath(\nu^2\pi r(\omega) + \gamma)}\,. \end{aligned} \tag{A13}$$

So,

$$\Upsilon^\dagger G(\omega)\Upsilon = \frac{(\omega-\omega_0+\iota\gamma)\times\left(\frac{\tau^2}{\omega-\omega_0+\iota\gamma}+t^2(R(\omega)-\iota\pi r(\omega))+2\nu\frac{R(\omega)-\iota\pi r(\omega)}{\omega-\omega_0+\iota\gamma}\tau t\right)}{(\omega-\omega_0-\nu^2R(\omega))+\iota(\nu^2\pi r(\omega)+\gamma)}$$
$$= \frac{\tau^2+2\nu(R(\omega)-\iota\pi r(\omega))\tau t+t^2(R(\omega)-\iota\pi r(\omega))((\omega-\omega_0)+\iota\gamma)}{(\omega-\omega_0-\nu^2R(\omega))+\iota(\nu^2\pi r(\omega)+\gamma)}$$
$$= \frac{(\tau^2+2\nu\tau tR+Rt^2(\omega-\omega_0)+\gamma t^2\pi r)+\iota(\gamma t^2R-\pi rt^2(\omega-\omega_0)-2\nu\tau t\pi r)}{(\omega-\omega_0-\nu^2R)+\iota(\nu^2\pi r+\gamma)}. \quad \text{(A14)}$$

The Raman susceptibility is determined by taking the imaginary part of Eq. (A14):

$$\Im[\Upsilon^\dagger G(\omega)\Upsilon] = \frac{N}{D}, \quad \text{(A15)}$$

with

$$D = (\omega-\omega_0-\nu^2R(\omega))^2+(\nu^2\pi r(\omega)+\gamma)^2 \quad \text{(A16)}$$

and

$$N = \Im\{[(\tau^2+2\nu\tau tR+Rt^2(\omega-\omega_0)+\gamma t^2\pi r)+\iota(\gamma t^2R-\pi rt^2(\omega-\omega_0)-2\nu\tau t\pi r)][(\omega-\omega_0-\nu^2R)-\iota(\nu^2\pi r+\gamma)]\}$$
$$= -[(\nu^2\pi r+\gamma)(\tau^2+2\nu\tau tR+Rt^2(\omega-\omega_0)+\gamma t^2\pi r)]+[((\omega-\omega_0)-\nu^2R)(\gamma t^2R-\pi rt^2(\omega-\omega_0)-2\nu\tau t\pi r)]. \quad \text{(A17)}$$

$$N = -\{[\underset{\cdots}{\nu^2\tau^2\pi r}+\overbrace{2\nu^3\tau t\pi rR}^{1.}+\overbrace{\nu^2t^2\pi r(\omega-\omega_0)R}^{2.}+\underline{\nu^2t^2\gamma(\pi r)^2}+\gamma\tau^2+2\gamma\nu\tau tR+\overbrace{\gamma t^2(\omega-\omega_0)R}^{3.}+\underline{\gamma^2t^2\pi r}]$$
$$+[\overbrace{-\gamma t^2(\omega-\omega_0)R}^{4.}+\underset{\cdots}{t^2\pi r(\omega-\omega_0)^2}+\underset{\cdots}{2\nu\tau t\pi r(\omega-\omega_0)}+\gamma\nu^2t^2R^2-\overbrace{\nu^2t^2\pi r(\omega-\omega_0)R}^{5.}-\overbrace{2\nu^3\tau t\pi rR}^{6.}]\}$$
$$= -t^2\left\{\underset{\cdots}{\pi r\left[\left(\omega-\omega_0\right)^2+2\nu\frac{\tau}{t}(\omega-\omega_0)+\nu^2\left(\frac{\tau}{t}\right)^2\right]}+\underline{\gamma\pi r(\nu^2\pi r+\gamma)}\right.$$
$$\left.+\gamma\left[\nu^2R^2+2\frac{\tau}{t}\nu R+\left(\frac{\tau}{t}\right)^2\right]\right\} \quad \text{(after 3. and 4., 2. and 5.,and 1. and 6. cancel)}$$
$$= -t^2\left\{\pi r(\omega)\left[\left(\omega-\omega_0+\nu\frac{\tau}{t}\right)^2+\gamma(\nu^2\pi r(\omega)+\gamma)\right]+\gamma\left(\nu R(\omega)+\frac{\tau}{t}\right)^2\right\}. \quad \text{(A18)}$$

Altogether,

$$\chi''(\omega) = t^2\frac{\pi r(\omega)\left[\left(\omega-\omega_0+\nu\frac{\tau}{t}\right)^2+\gamma(\nu^2\pi r(\omega)+\gamma)\right]+\gamma\left(\nu R(\omega)+\frac{\tau}{t}\right)^2}{(\omega-\omega_0-\nu^2R(\omega))^2+(\nu^2\pi r(\omega)+\gamma)^2}. \quad \text{(A19)}$$

2. Comparison to the parameterized Fano lineshape

In the limit $\gamma \to 0$, corresponding to the δ-function-like discrete state described by Fano, expression (A19) for the Raman susceptibility of the coupled modes,

$$\lim_{\gamma\to 0}\left\{\frac{\chi''(\omega)}{\pi r(\omega)t^2}\right\} = \frac{\left(\omega-\omega_0+\nu\frac{\tau}{t}\right)^2}{(\omega-\omega_0-\nu^2R(\omega))^2+(\nu^2\pi r(\omega))^2}$$
$$= \frac{1}{(\nu^2\pi r(\omega))^2}\frac{\left(\omega-\omega_0+\nu\frac{\tau}{t}\right)^2}{1+\left(\frac{\omega-\omega_0-\nu^2R(\omega)}{\nu^2\pi r(\omega)}\right)^2}, \quad \text{(A20)}$$

can be compared to the classical expression, parameterized by ε and q as described by Klein.[5] By setting $\Omega = \omega_0+\nu^2R$ and $\Gamma_\varepsilon = \pi\nu^2r$, we find that Eq. (A20) corresponds to the classical equation if $\varepsilon = \frac{\omega-\Omega}{\Gamma_\varepsilon}$. With $\varepsilon = -\cot\Delta$, it follows that $\Delta = -\text{arc}\cot[\frac{\omega-\Omega}{\Gamma_\varepsilon}] = -\text{arc}\cot[\frac{\omega-\omega_0-\nu^2R(\omega)}{\nu^2\pi r(\omega)}]$ for the phase shift Δ. The ratio q is determined from the condition

$$q+\frac{\omega-\omega_0-\nu^2R(\omega)}{\nu^2\pi r(\omega)} \stackrel{!}{=} \frac{1}{\nu^2\pi r(\omega)}\left(\omega-\omega_0+\nu\frac{\tau}{t}\right),$$
$$\text{so that } q = \frac{\nu\frac{\tau}{t}+\nu^2R(\omega)}{\nu^2\pi r(\omega)} = \frac{\frac{1}{\nu}\frac{\tau}{t}+R(\omega)}{\pi r(\omega)}. \quad \text{(A21)}$$

3. Analytical expression for the continuum

We approximate the constant continuum by a Lorentzian with a very large linewidth. This choice of $r(\omega)$ allows us to model an almost flat continuum in an exceedingly wide frequency range and, at the same time, to have an expression

that yields a Hilbert integral in analytical form:

$$r(\omega) \sim \frac{\Gamma_C}{(\omega-\omega_C)^2+\Gamma_C^2}, \tag{A22}$$

so that $r(\omega) = a\widetilde{r}(\omega)$. Here, an additional parameter a, the experimentally observed amplitude of the electronic continuum, is introduced. For the real part of the electronic Green's function as it is used in Eq. (A19) this gives

$$\begin{aligned} R(\omega) &= -H_T[r(\omega)] = -aH_T[\widetilde{r}(\omega)] \\ &= a\int \frac{\widetilde{r}(\omega')}{\omega-\omega'}d\omega' = a\widetilde{R}(\omega), \end{aligned} \tag{A23}$$

with

$$\widetilde{R}(\omega) = \frac{\omega-\omega_C}{(\omega-\omega_C)^2+\Gamma_C^2}. \tag{A24}$$

In the above equations, ω_C is the central frequency of the Lorentzian shape and Γ_C its linewidth. Since the Raman susceptibility of the hybridized lineshape needs to be fitted to the experimental data, it is important to realize which parameters in Eq. (A19) are in fact independent, once the equation is adjusted for the phenomenological input of the experimentally observed electronic continuum, that is after the introduction of the amplitude a. With the electronic Green's function approximated by expressions (A22) and (A24),

$$\chi''(\omega) = \frac{at^2\pi\widetilde{r}(\omega)\left[\left(\omega-\omega_0+\nu\frac{\tau}{t}\right)^2+\gamma(a\nu^2\pi\widetilde{r}(\omega)+\gamma)\right]+\gamma(a\nu t\widetilde{R}(\omega)+\tau)^2}{(\omega-\omega_0-a\nu^2\widetilde{R}(\omega))^2+(a\nu^2\pi\widetilde{r}(\omega)+\gamma)^2}. \tag{A25}$$

By observing that

$$a\nu t = \nu\frac{\tau}{t}\cdot at^2 \quad \text{and} \quad a\nu^2 = \nu^2\frac{\tau^2}{t^2}\cdot at^2\cdot\frac{1}{\tau^2},$$

it is found that there are only three independent parameters: the amplitude of the continuum $A = at^2$, the ratio of the phonon and continuum transition matrix elements weighted by the coupling strength $B = \nu\frac{\tau}{t} \equiv \tilde{\nu}$, and the square of the phonon transition matrix element $C = \tau^2$. Accordingly, the fitting function is written as

$$\chi''(\omega) = \frac{A\pi\widetilde{r}(\omega)\left[(\omega-\omega_0+B)^2+\gamma\left(\frac{AB^2}{C}\pi\widetilde{r}(\omega)+\gamma\right)\right]+\gamma(AB\widetilde{R}(\omega)+C^{\frac{1}{2}})^2}{\left(\omega-\omega_0-\frac{AB^2}{C}\widetilde{R}(\omega)\right)^2+\left(\frac{AB^2}{C}\pi\widetilde{r}(\omega)+\gamma\right)^2}. \tag{A26}$$

This is the expression that is coded in a fitting module of a commercial mathematical package. It is important to note that due to the stated choice of the Green's functions our description remains phenomenological. However, if analytic expressions for the Green's functions describing the local phononic mode and the continuous electronic excitations from impurity levels to the conduction band could be found based on a microscopic physical model, then this exercise can be readily extended to develop a microscopic theory of the Breit-Wigner-Fano interference in resonant Raman scattering.

*Corresponding author: aleksej.mialitsin@nrel.gov

[1] H. M. Cheong, Y. Zhang, A. Mascarenhas, and J. F. Geisz, Phys. Rev. B **61**, 13687 (2000).

[2] A. Mascarenhas, M. J. Seong, S. Yoon, J. C. Verley, J. F. Geisz, and M. C. Hanna, Phys. Rev. B **68**, 233201 (2003).

[3] A. J. Ptak, D. J. Friedman, Sarah Kurtz, and R. C. Reedy, J. Appl. Phys. **98**, 094501 (2005).

[4] U. Fano, Phys. Rev. **124**, 1866 (1961).

[5] M. V. Klein, *Light Scattering in Solids I*, in *Topics in Applied Physics*, Vol. 8, 2nd ed. (Springer, Berlin, Heidelberg, 1983), Chap. 4.

[6] G. Blumberg, M. V. Klein, L. Boejesson, R. Liang, and W. N. Hardy, J. Supercond. **7**, 445 (1994).

[7] A. Mialitsin, J. Phys. Chem. Sol. **72**, 568 (2011).

[8] A. Mialitsin, J. S. Kim, R. K. Kremer, and G. Blumberg, Phys. Rev. B **79**, 064503 (2009).

[9] H. F. Liu, N. Xiang, S. Tripathy, and S. J. Chua, J. Appl. Phys. **99**, 103503 (2006).

[10] A. M. Mintairov, P. A. Blaganov, V. G. Melchin, N. N. Fadeev, J. L. Merz, Y. Qiu, S. A. Nikishin, and H. Temkin, Phys. Rev. B **56**, 15836 (1997).

[11] G. Bachelier, A. Mlayah, M. Cazayous, J. Groenen, A. Zwick, H. Carrère, E. Bedel-Pereira, A. Arnoult, A. Rocher, and A. Ponchet, Phys. Rev. B **67**, 205325 (2003).

[12] Kanti Jain, Shui Lai, and Miles V. Klein, Phys. Rev. B **13**, 5448 (1976).

[13] Sample no. N829, OVPE grown, $x = 0.78\%$: by M. Hanna.

[14] D. G. Thomas, J. J. Hopfield, and C. J. Frosch, Phys. Rev. Lett. **15**, 857 (1965).

[15] D. G. Thomas and J. J. Hopfield, Phys. Rev. **150**, 680 (1966).

[16] P. J. Colwell and M. V. Klein, Phys. Rev. B **6**, 498 (1972).

[17] N. Gonzalez Szwacki and P. Bogusławski, Phys. Rev. B **64**, 161201 (2001).

[18] D. N. Zubarev, Usp. Fiz. Nauk SSSR **71**, 71 (1960) [Sov. Phys. Usp. **3**, 320 (1960)].